Solid State Communications 192 (2014) 47–50

Contents lists available at ScienceDirect

Solid State Communications

journal homepage: www.elsevier.com/locate/ssc

Surface impedance in the antiferromagnetic and superconducting states of underdoped $BaFe_{1.93}Ni_{0.07}As_2$ crystals

M. Saint-Paul [a,*], C. Guttin [a], A. Abbassi [b], Zhao-Sheng Wang [a,c,1], Huiqian Luo [c], Xingye Lu [c], Cong Ren [c], Hai-Hu Wen [c,d], K. Hasselbach [a]

[a] Université Grenoble, CNRS, Institut Néel 166, F 38042 Grenoble Cedex 9, France
[b] Faculté des Sciences et Techniques de Tanger, BP 416 Tanger, Université Abdelmalek Essaâdi, Morocco
[c] Institute of Physics and National Laboratory for Condensed Matter Physics, Chinese Academy of Sciences, P.O. Box 603, Beijing 100190, China
[d] National Laboratory for Solid State Microstuctures, Departement of Physics, Nanjing University, 210093 Nanjing, China

ARTICLE INFO

Article history:
Received 31 January 2014
Received in revised form
5 May 2014
Accepted 15 May 2014
by P. Sheng
Available online 22 May 2014

Keywords:
A. Pnictides
D. Superconductivity
E. Surface impedance

ABSTRACT

Measurements of the real R and imaginary X parts of the surface impedance were performed in underdoped $BaFe_{1.93}Ni_{0.07}As_2$ crystals in the frequency range 10 MHz–1.5 GHz. The establishment of the antiferromagnetic order at $T_N \sim 50$ K gives rise to anomalous increase of electron scattering time. Drude type conductivity yields X and R differ from each other. The increase of the real conductivity σ_1 in the superconducting state is attributed to a rapid decrease of the quasiparticle scattering time. This result gives evidence of coexistence of superconductivity and antiferromagnetism.

1. Introduction

The underdoped $BaFe_{1.93}Ni_{0.07}As_2$ exhibits a structural transition at $T_S \sim 70$ K, an antiferromagnetic transition at $T_N \sim 50$ K and a superconducting transition at $T_C \sim 16$ K [1–4]. NMR measurements give clear evidence of coexistence of superconductivity and antiferromagnetism [1]. The spin-lattice relaxation shows a critical slowing down around T_N and a further strong decrease around the superconducting transition. A number of surface impedance measurements have been published on iron based superconductors. They give information on London penetration depth and quasiparticle scattering [5–9]. The power temperature dependence of the London penetration depth in the *ab* plane $\lambda(T)-\lambda(0)\sim T^n$ with $n\sim 2$–2.8 is attributed to pair breaking scattering in the so-called $s^{\pm}$ superconductivity [5–8]. The sharp increase of the real part of the conductivity below T_c was explained by a rapid decrease of the quasiparticle scattering rate for the optimally Co and Ni doped crystals [7–9].

Here we report surface impedance measurements on underdoped $BaFe_{1.93}Ni_{0.07}As_2$ in the frequency range 10 MHz–1.5 GHz. Careful analysis of the impedance measurements permits us to observe that the real R and imaginary X parts of the surface impedance of underdoped $BaFe_{1.93}Ni_{0.07}As_2$ differ from each other in the antiferromagnetic state. A large decrease of the scattering rate τ^{-1} of the charge carriers produced by the establishment of the antiferromagnetic order gives a complex Drude conductivity $\sigma=\sigma_0/(1+j\omega\tau)$ where ω is the measuring angular frequency with $\omega\tau\sim 1$ [10]. Complex conductivity induces $R\neq X$.

2. Experiment

The crystals were grown using a Fe/Ni–As self flux method, details are given in [4]. The samples are platelike with the plates perpendicular to the crystallographic axis *c*. The same surface impedance measurement technique was used for optimally and over doped $BaFe_{2-x}Ni_xAs_2$ crystals in reference [9]. The samples are placed inside a copper coil situated at the end of a coaxial line. The radio frequency magnetic field is applied parallel to the *ab* plane. Non resonant measurements of the resistance and inductance of the coil were performed with an automated impedance analyzer Agilent 4395 in the frequency range 10–100 MHz. Resonant measurements of the LC resonant frequency, $L=0.2$ μH, $C=50$ fF quality factor 80, were performed at 1.5 GHz with a Hewlett Packard 8720B network analyzer. Resistance and inductance were measured separately in the absence of the sample and were subtracted from measurements with the sample present.

* Corresponding author.
E-mail address: Michel.saint-paul@neel.cnrs.fr (M. Saint-Paul).
[1] Present address: Hochfeld-Magnetlabor Dresden, Helmholtz-Zentrum Dresden-Rossendorf, D-01314 Dresden, Germany.

http://dx.doi.org/10.1016/j.ssc.2014.05.009
0038-1098/

The inductance of the coil is given by [11]

$$Z = R_0 + \frac{k^2 L_0 L_2 \omega^2 R}{|R + j(X + L_2\omega)|^2} + j\left[L_0 - \frac{k^2 L_0 L_2 \omega\{X + L_2\omega\}}{|R + j(X + L_2\omega)|^2}\right]\omega \quad (1)$$

where R and X are the real and imaginary parts of the surface impedance of the sample, R_0 and $L_0 \sim 0.2$ μH, are the resistance and inductance of the empty coil and ω is the angular frequency. Coupling k and geometrical L_2 factors were evaluated from measurements at high temperatures ~ 100 K, $k^2 \sim 0.1$ and $L_2 \sim 0.6$ nH. R and X are deduced from Eq. (1). At high temperatures

$$Z = \sqrt{\frac{j\mu_0\omega}{\sigma_{HT}}} \quad \text{with} \quad X_{HT} = R_{HT} = \sqrt{\mu_0 \rho_{dc}\omega/2} \quad (2)$$

where μ_0 is the magnetic permeability of vacuum and $\sigma_{HT} = 1/\rho_{dc}$ is the conductivity at ~ 100 K , $\rho_{dc} \sim 0.2$ mΩ cm is the measured dc resistivity [4]. At 100 K, a skin depth $\delta = \sqrt{2/\mu_0\sigma_{HT}\omega} \sim 50$ μm is estimated at 100 MHz.

3. Results and discussion

The temperature dependence of R and X normalized to the value R_{HT} measured at 100 K are shown in Figs. 1 and 2. X and R differ from each other in the superconducting state below T_c and in the antiferromagnetic state below the Neel transition $T_N \sim 50$ K. Meanwhile $X = R$ is found in the high temperature range above T_N.

3.1. Antiferromagnetic state in the temperature range $T_C < T < T_N$

X and R differ from each other in the antiferromagnetic state. An increase of the electron scattering time τ_m in the antiferromagnetic state originates a complex Drude type conductivity $\sigma = \sigma_0/(1 + j\omega\tau_m)$ [10], where σ_0 is the dc conductivity

Surface impedance is now given by

$$Z = R + jX = \sqrt{\frac{j\mu_0(1 + \omega\tau_m)\omega}{\sigma_0}} \quad (3)$$

The parameters $\omega\tau_m$ and σ_0/σ_{HT} are deduced from the measurements of X/R_{HT} and R/R_{HT} using the following relations deduced from Eq. (3)

$$\frac{\sigma_0}{\sigma_{HT}} = \frac{R_{HT}}{R}\frac{R_{HT}}{X} \quad \text{and} \quad \omega\tau_m = \frac{(X/R_{HT})^2 - (R/R_{HT})^2}{2(R/R_{HT})(X/R_{HT})} \quad (4)$$

The resulting $\omega\tau_m$ and σ_0/σ_{HT} parameters are shown in Figs. 1 and 2. For $T > T_N$, $\omega\tau_m = 0$ is consistent with $X_{HT} = R_{HT}$ in the high temperature state. In the antiferromagnetic state τ_m increases with decreasing temperature from T_N to 20 K. A saturating value of $\omega\tau_m \sim 0.12$, 0.26 and 0.5 is found around 20 K at 10, 20 and 100 MHz. Within our experimental resolution no difference between R and X is detected at 1.5 GHz in the temperature range above T_c. For Ni doping level $x = 0.075$ $\omega\tau_m \sim 0.1$ is obtained at 20 and 100 MHz (Fig. 2).

The temperature dependence of the relaxation rate τ_m^{-1} deduced from Fig. 1 is shown in Fig. 3. Increase of τ_m^{-1} with

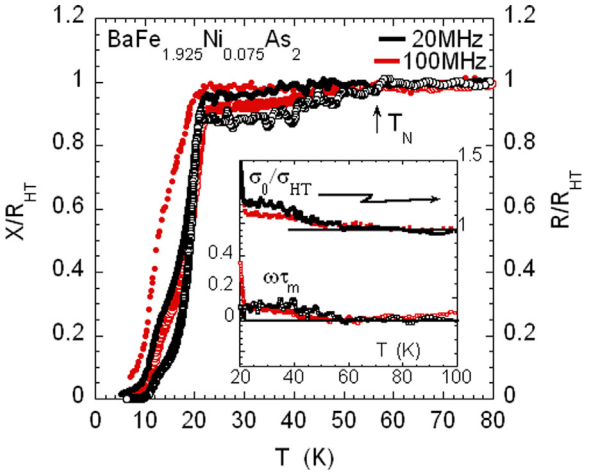

Fig. 2. Temperature variation of X/R_{HT} (filled symbols) and R/R_{HT} (open symbols) of surface impedance, R_{HT} is obtained at 100 K for the underdoped $BaFe_{1.925}Ni_{0.075}As_2$ crystals at 20 MHz (black), 100 MHz (red). Inset: Temperature dependence of σ_0/σ_{HT} normalized to the value σ_{HT} at 100 K and of $\omega\tau_m$ with $\omega = 2\pi F$, $F = 20$ and 100 MH.(For interpretation of the references to color in this figure legend, the reader is referred to the web version of this article.)

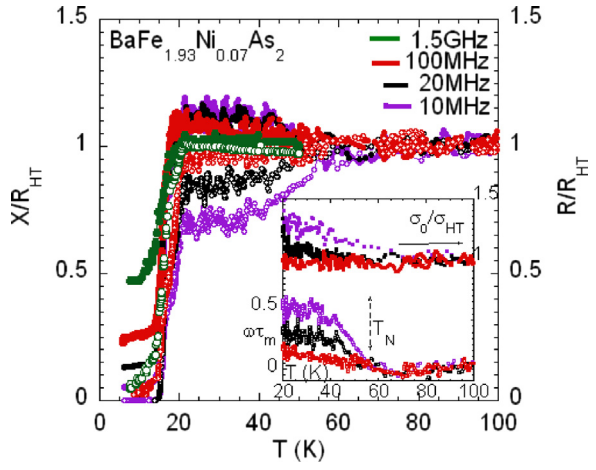

Fig. 1. Temperature variation of X/R_{HT} (filled symbols) and R/R_{HT} (open symbols) of surface impedance, R_{HT} is obtained at 100 K for the underdoped $BaFe_{1.93}Ni_{0.07}As_2$ crystals at 10 MHz(violet), 20 MHz (black), 100 MHz (red), 1.5 GHz (green). Inset: Temperature dependence of σ_0/σ_{HT} normalized to the value σ_{HT} at 100 K and of $\omega\tau_m$ with $\omega = 2\pi F$, $F = 10$, 20 and 100 MHz. (For interpretation of the references to color in this figure legend,the reader is referred to the web version of this article.)

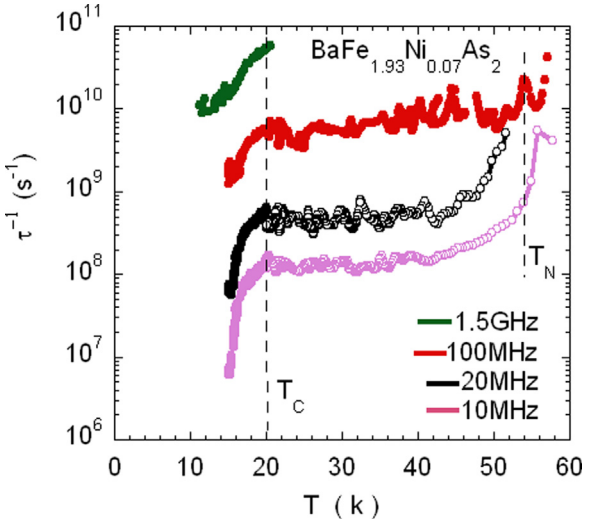

Fig. 3. Temperature dependence of the electron scattering rate τ_m^{-1} in the temperature range $20\text{ K} < T < T_N$ and of the quasiparticle scattering rate τ^{-1} deduced from the conductivity σ_1 in the superconducting state for the underdoped $BaFe_{1.93}Ni_{0.07}As_2$. At each frequency we take $\tau^{-1}(20\text{ K}) = \tau_m^{-1}(20\text{ K})$.

increasing frequency or decreasing skin depth δ is found. Such an effect could be attributed to an additional scattering of electrons by surface defects whose contribution increases with the decreasing skin depth. Conductivity σ_0 increases slightly with the decreasing temperature from T_N to 20 K Figs. 1 and 2.

3.2. Superconducting state

Our resistance measurements are well resolved in the vicinity of the superconducting transition.

But below 15 K our experimental resolution is not sufficient to extract the intrinsic resistance.

Surface impedance Z is related to the real σ_1 and imaginary σ_2 parts of the conductivity:

$$Z = R + jX = \sqrt{\frac{j\mu_0\omega}{\sigma_1 - j\sigma_2}} \tag{5}$$

σ_1 and σ_2 are normalized to the value $\sigma_1(20\text{ K}) = \sigma_0(20\text{K}) \sim \sigma_{HT}$ at 20 K.

The real σ_1 and imaginary σ_2 parts are given by inverting Eq. (5).

$$\frac{\sigma_1}{\sigma_{HT}} = \frac{4RX/R_{HT}^2}{[(R/R_{HT})^2 + (X/R_{HT})^2]^2} \quad \frac{\sigma_2}{\sigma_{HT}} = 2\frac{(X/R_{HT})^2 - (R/R_{HT})^2}{[(R/R_{HT})^2 + (X/R_{HT})^2]^2} \tag{6}$$

Temperature dependences of σ_1/σ_{HT} and $\sigma_2/\sigma_2(0)$, with $\sigma_2(0) = \sigma_2(T=0)$ are shown in Fig. 4.

The conductivity $\sigma_2/\sigma_2(0)$ is related to the London penetration depth [4–9] and follows a T^2 temperature dependence:

$$\frac{\sigma_2}{\sigma_2(0)} = \frac{\lambda(0)^2}{\lambda(T)^2} \quad \text{and} \quad \frac{\sigma_2}{\sigma_2(0)} \approx 1 - \left(\frac{T}{T_C}\right)^2 \tag{7}$$

The conductivity $\sigma 1$ increases with decreasing temperature below $T_C \sim 16$ K to a maximum of about 2–10 times its normal value and this maximum decrease with increasing frequency from 10 MHz to 1.5 GHz. The strong rise in the conductivity $\sigma 1$ below T_C results from a temperature dependent scattering rate decreasing rapidly with temperature [7–9]. A smaller broad variation is observed between 16 K and 20 K. The phenomenological two fluid model is used to extract the quasiparticle scattering time τ [12,13]. The superconducting density, n_S is related to the London penetration depth $n_S = \lambda(0)2/\lambda 2$. The normal density n_N is given by $n_N = 1 - n_S$, the total carrier density being 1. It results that the temperature dependence of n_N in the underdoped $BaFe_{2-x}Ni_xAs_2$ crystals follows the $(T/T_C)2$ temperature dependence. σ_1 is proportional to the product $n_N\tau$ [12] which gives, $\sigma_1 \sim (T/T_C)2\tau$. Consequently scattering rate τ^{-1} is given by

$$\frac{\tau^{-1}(T)}{\tau^{-1}(T_C)^{-1}} = \left(\frac{T}{T_C}\right)^2 \frac{\sigma^{-1}{}_1(T)}{\sigma_1{}^{-1}(T_C)} \tag{8}$$

where $\tau^{-1}(T_C)$ is the scattering rate at $T_C \sim 16$ K.

In the temperature range 16–20 K (Fig. 4) $\sigma_2 \sim 0$ gives $n_N \sim 1$ and Eq. (8) is reduced to

$$\frac{\tau^{-1}(T)}{\tau^{-1}(20\text{ K})} = \frac{\sigma_1{}^{-1}(T)}{\sigma_1^{-1}(20\text{ K})} \tag{9}$$

At 20 K the scattering rate $\tau^{-1}(20\text{K})$ is equal to $\tau_m^{-1}(20\text{ K})$ which is the relaxation rate determined with Eq. (4). The scattering rates deduced at the different frequencies are shown in Fig. 3. At 1.5 GHz, $\tau^{-1}(20\text{ K}) \sim 6 \times 10^{10}$ was arbitrary taken.

Finally significant decrease of the electron scattering rate is observed around T_N (Fig. 3) when magnetic order sets in. Below T_C, strong decrease of the quasiparticle scattering rate is found in the superconducting state. This result is similar to the temperature dependence of $1/T_1$ [1]. Evidence for coexistence of superconductivity and antiferromagnetism is given.

The superconducting transition is quite broadened in the temperature range 16–20 K for the underdoped crystals in contrast with the optimally and over doped crystals [9]. This result is in agreement with the broad elastic anomaly of the C33 mode observed with the same crystals [14]. The purely electronic effects are strongly affected by structural instabilities near the superconducting transition in the Ni and Co underdoped $BaFeAs_2$ crystals [15].

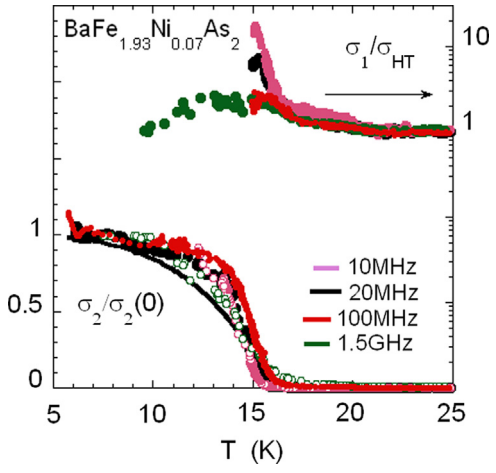

Fig. 4. Temperature dependence of the real σ_1/σ_{HT} (filled symbols) and imaginary σ_2/σ_{HT} (open symbols) parts of the effective conductivity, σ_{HT} is the conductivity at 100 K, for underdoped $BaFe_{1.93}Ni_{0.07}As_2$ at 10 MHz, 20 MHz,100 MHz and 1.5 GHz. Solid line $\sigma_2/\sigma_2(0)$ is calculated with $1-(T/16)^2$.

4. Conclusion

Establishment of antiferromagnetic order in underdoped $BaFe_{1.93}Ni_{0.07}As_2$ crystals gives rise to an anomalous increase of electron scattering time which leads that the real and imaginary parts of complex surface impedance differ from each other $X > R$. The increase of the real conductivity $\sigma_1$in the superconducting state is attributed to a strong decrease of the quasiparticle scattering time. This result gives evidence for coexistence of superconductivity and antiferromagnetism.

References

[1] R. Zhou, Z. Li, J. Yang, D.L Sun, C.T. Lin, Guo-qing Zheng, Nat. Commun. 4 (2013) 2265.
[2] Xingye Lu, H. Gretarsson, Rui Zhang, Xuerong Liu, Huiqian Luo, Wei Tian, Mark Laver, Z. Yamani, Young-June Kim, A.H. Nevidomskyy, Qimiao Si, Pengcheng Dai, Phys. Rev. Lett. 110 (2013) 257001.
[3] Huiqian Luo, Rui Zhang, Mark Laver, Zahra Yamani, Meng Wang, Xingye Lu, Miaoyin Wang, Yanchao Chen, Shiliang Li, Sung Chang, Jeffrey W. Lynn, Pengcheng Dai, Phys. Rev. Lett. 108 (2012) 247002.
[4] Yanchao Chen, Xingye Lu, Meng Wang, Huiqian Luo, Shiliang Li, Supercond. Sci. Technol. 24 (2011) 065004–065008.
[5] R. Prozorov, V.G. Kogan, Rep. Prog. Phys. 74 (2011) 1245051–12450520.
[6] P. Rodière, T. Klein, L. Lemberger, K. Hasselbach, A. Demuer, J. Kacmarcik, Z. S. Wang, H.Q. Luo, X.Y. Lu, H.H. Wen, F. Gucmann, C. Marcenat, Phys. Rev. B 85 (2012) 214506.
[7] A. Barannik, N.T. Cherpak, M.A. Tanatar, S. Vitusevich, V. Skresanov, P.C. Canfield, R. Prozorov, Phys. Rev. B 87 (2013) 014506.
[8] J.S. Bobowski, J.C. Baglo, James Day, P. Dosanjh, Rinat Ofer, B.J. Ramshaw, Ruixing Liang, D.A. Bonn, W.N. Hardy, Huiqian Luo, Zhao-Sheng Wang, Lei Fang, Hai-Hu Wen, Phys. Rev. B 82 (2010) 094520.
[9] M. Saint-Paul, C. Guttin, A. Abbassi, Zhao-Sheng wang, Huiqian Luo, Xingye Lu, Cong Ren, Hai-Hu Wen, K. Hasselbach, Solid State Commun. 185 (2014) 10–13.
[10] Durga P. Choudhury, H. Srikanth, S. Sridhar, P.C. Canfield, Phys. Rev. 58 (1998) 14490.
[11] Yann Le Bihan, NDT E Int. 36 (2003) 297–302.

[12] M.R. Trunin, A.A. Golubov, in: N.M. Plakida (Ed.), Spectroscopy of High Temperature Superconductors, Taylor & Fracis Ltd. (Eds), London United Kingdom, 2003, pp. 159–233.
[13] D.A. Bonn, Ruixing Liang, T.M. Riseman, D.J. Baar, D.C. Morgan, Kuan Zhang, P. Dosanjh, T.L. Duty, A. MacFarlane, G.D. Morris, J.H. Brewer, W.N. Hardy, C. Kallin, A.J. Berlinsky, Phys. Rev. B 47 (1993) 11314.
[14] M. Saint-Paul, A. Abbassi, Zhao-Sheng Wang, Huiqian Luo, Xingye Lu, Cong Ren, Hai-Hu Wen, K. hasselbach, Physica C 483 (2012) 207–212.
[15] Masahito Yoshizawa, Shalamujiang Simayi, Kohei Sakano, Yoshiki Nakanishi, Kunihiro Kihou, Chul-Ho Lee, Akira Iyo, Hiroshi Eisaki, Masamichi Nakajima, Shin-Ichi Uchida, Solid State Commun. 152 (2012) 680–687.